EFFICIENT NUMERICAL SIMULATION OF UNSTEADY CAVITATING FLOWS USING THERMODYNAMIC TABLES

F. Khatami
University of Twente, the Netherlands

A. H. Koop
Marin, the Netherlands

E. T. A. van der Weide
University of Twente, the Netherlands

H. W. M. Hoeijmakers
University of Twente, the Netherlands

SUMMARY

A computational method based on the Euler equations for unsteady flow is employed to predict the structure and dynamics of unsteady sheet cavitation as it occurs on stationary hydrofoils, placed in a steady uniform inflow. An equilibrium cavitation model is employed, which assumes local thermodynamic and mechanical equilibrium in the two-phase flow region. Furthermore, the phase transition does not depend on empirical constants in this model.

In order to be able to predict the dynamics of the pressure waves, the fluid is considered as a compressible medium by adopting appropriate equations of state for the liquid phase, the two-phase mixture and the vapor phase of the fluid. When these thermodynamic relations are used directly in the computational method, it was found that over 90% of the computational time was spent by computations associated with these closure relations.

Therefore, in this paper this approach is replaced by using precomputed thermodynamic tables, containing the same information. It will be shown that the thermodynamic functions for the liquid, vapor, and mixture phases are consistent and have unique values in all the phases. Accordingly, a unique table can be prepared for any of the thermodynamic variables $\{p, T, c, \alpha\}$, i.e. pressure, temperature, speed of sound, and vapor void fraction, covering all three phases in each table. Based on uniqueness property of the tables, the thermodynamic state can be characterized without any need for determining the flow phase, although it has been stored in a table for post processing purposes (and for later viscous simulations).

To show that this approach is beneficial, results on sheet cavitation for the NACA0015 hydrofoil will be presented. The results clearly show the shedding of a sheet cavity and the strong pressure pulses, originating from the collapse of shed vapor structures. The usage of the tables leads to a speed-up of the computations of approximately a factor of 10.

NOMENCLATURE

p_∞ [Pa]	Free-stream pressure
ρ_∞ [kg m^{-3}]	Free-stream density
U_∞ [m s^{-1}]	Free-stream velocity
V [m^3]	Volume of the fluid
V_v [m^3]	Volume of the vapor
p_{sat} [Pa]	Saturation pressure
$\rho_{v,sat}$ [kg m^{-3}]	Saturation vapor density
$\rho_{l,sat}$ [kg m^{-3}]	Saturation liquid density
$\sigma = \frac{p_\infty - p_{sat}(T)}{1/2\rho_\infty U_\infty^2}$	Cavitation number
$\alpha = \frac{V_v}{V} = \frac{\rho - \rho_{l,sat}(T)}{\rho_{v,sat}(T) - \rho_{l,sat}(T)}$	Void fraction

INTRODUCTION

Cavitation is an unsteady process which involves formation and collapse of vapor cavities in a liquid. Vapor cavities appear in regions where the liquid pressure drops below the saturation pressure and afterwards collapse in regions with higher pressure. There are many applications involving cavitating flows, some examples are in technical applications such as pumps, turbines, ship propellers, fuel injection systems, bearings, and in medical sciences such as lithotripsy treatment and the flow through artificial heart valves.

The implosions and explosions of vapor regions of cavitating flows in hydraulic systems may cause a number of problems. These include vibration and noise, surface erosion in the case of developed cavitation, and deteriorating the performance of the system such as lift reduction and increase in drag of a foil and loss of turbomachinary efficiency. However, besides the harmful effects, cavitation is used in some industrial processes to produce high pressure peaks and apply it for cleaning of surfaces, dispersion of particles in a liquid, production of emulsions etc. Cavitation cannot be avoided in many applications due to a demand for high efficiency or is an essential part of the design in some other applications. Hence to be able to control the effects of cavitation, it is essential to understand the driving mechanisms of this phenomenon.

Proceedings of the Eighth International Symposium on Cavitation (CAV 2012)
Edited by Claus-Dieter OHL, Evert KLASEBOER, Siew Wan OHL, Shi Wei GONG and Boo Cheong KHOO.

ISBN: 978-981-07-2826-7 :: doi:10.3850/978-981-07-2826-7_098

In this paper a computational method is presented to simulate an unsteady cavitation computation, which is a continuation of the work performed by Schmidt *et al.* [1] and Koop *et al.* [2, 3]. The method is applied to an unsteady sheet cavitation, for which an inviscid compressible flow is assumed together with appropriate thermodynamic equations of state i.e. Tait's equation for the liquid phase, a perfect gas for the vapor phase, and an equilibrium model for the mixture phase. These thermodynamic equations are highly nonlinear and especially for the mixture phase computationally costly. E.g. a profiling of the code used by Koop [3] showed that roughly 90% of the computational work was carried out in the routines for these thermodynamic relations. As an alternative, we have prepared a set of thermodynamic tables, which eliminate the iterative steps for solving thermodynamic equations. Using this approach a speed up of approximately a factor 10 can be obtained.

This paper is organized as follows. First the physical model is described in section 1, including the thermodynamic closure relations. This is followed by the construction of the tables, section 2, and the discretization method, section 3. Results are presented in section 4 and this paper ends with the conclusions and a description of future work, section 5.

1 PHYSICAL MODELING

In order to model the sheet cavitation some assumptions must be used. Since the main structures of sheet cavitation are dominantly inertia driven, the flow is considered inviscid. One of the main issues in numerical simulation of unsteady cavitating flow is the simultaneous treatment of two very different flow regions, i.e. the (nearly) incompressible flow of pure liquid in most of the flow domain with a fluid of relatively high density and the highly compressible flow of (pure) vapor with very low density in a small part of the flow domain. To be able to capture the shock waves, the flow is considered compressible. Based on the model from Saurel *et al.* [4] and Schmidt *et al.* [1] the equilibrium cavitation model is adopted. In this model the two-phase flow regime is assumed to be a homogeneous mixture of liquid and vapor. Furthermore relative velocities between the liquid and vapor parts are neglected, and local pressure and temperature equilibrium are assumed. In other words, the two-phase flow is in mechanical and thermodynamic equilibrium. Based on these assumptions, appropriate thermodynamic equations need to be introduced to cover all the possible states. The equations of state must preserve the hyperbolic nature of the resulting system of equations so that the pressure waves in the fluid can be represented. The governing equations of motion for the model described above are the Euler equations which in integral conservation form are given by

$$\frac{\partial}{\partial t}\iiint_{\Omega}\mathbf{U}\,\mathrm{d}\Omega+\iint_{\Gamma=\partial\Omega}\vec{\mathbf{F}}\left(\mathbf{U}\right).\mathbf{n}\,\mathrm{d}\Gamma=0. \tag{1}$$

Here it is assumed that Ω is a bounded polygon domain in $\mathbb{R}^3$ with boundary $\partial\Omega$, the vector $\mathbf{U}$ denotes the vector of conservative variables, that is $\mathbf{U}=[\rho,\rho u,\rho v,\rho w,\rho E]$ and $\vec{\mathbf{F}}\left(\mathbf{U}\right)\cdot\mathbf{n}$ is the normal component of the inviscid flux vector in Cartesian coordinates

$$\vec{\mathbf{F}}\left(\mathbf{U}\right).\mathbf{n}=\begin{bmatrix}\rho\hat{u}\\ \rho\hat{u}u+pn_x\\ \rho\hat{u}v+pn_y\\ \rho\hat{u}w+pn_z\\ \rho\hat{u}H\end{bmatrix}, \tag{2}$$

where $\hat{u}$ is the velocity normal to the surface Γ that is $\hat{u}=\mathbf{u}\cdot\mathbf{n}$. Furthermore H denotes the total enthalpy

$$H=E+\frac{p}{\rho}=h+\frac{1}{2}\mathbf{u}.\mathbf{u}, \tag{3}$$

where E and h are the total energy and specific static enthalpy, $h=e+p/\rho$, respectively. E is defined as

$$E=e+\frac{1}{2}\mathbf{u}.\mathbf{u}, \tag{4}$$

where e denotes the specific internal energy.

The unknowns for the system of equations are $\{\rho,u,v,w,e,p,T\}$, To close the system of equations two additional equations are needed, which are given by the thermodynamics, namely $\rho=\rho\left(p,T\right)$ and $h=h\left(p,T\right)$. These relations must be known for the liquid, vapor, and mixture phases. In the following equations of state are given. The expressions for liquid, vapor, and saturation densities are denoted by subscripts l, v, and sat, respectively. The speed of sound within each state is obtained from [2]

$$c^2=\frac{\rho\left(\frac{\partial h}{\partial T}\right)_p}{\rho\left(\frac{\partial\rho}{\partial p}\right)_T\left(\frac{\partial h}{\partial T}\right)_p+\left(\frac{\partial\rho}{\partial T}\right)_p\left\{1-\rho\left(\frac{\partial h}{\partial p}\right)_T\right\}}. \tag{5}$$

LIQUID PHASE

Following by Saurel *et al.* [4], a modified Tait equation of state is used which describes the liquid pressure in terms of density and temperature

$$p_l\left(\rho_l,T_l\right)=K_0\left[\left(\frac{\rho_l}{\rho_{l,sat}}\right)^N-1\right]+p_{sat}, \tag{6}$$

where for water $K_0=3.3\times10^8\,Pa$ and $N=7.15$ are constants. An approximate caloric equation of state, given by

$$e_l\left(\rho_l,T_l\right)=e_l\left(T_l\right)=C_{vl}\left(T_l-T_0\right)+e_{l0}, \tag{7}$$

is adopted, which is based on [2] and provides a good approximation. The constants in the above equation with their corresponding values for water are defined as: $C_{vl}=4180\,\mathrm{J\,kg^{-1}\,K^{-1}}$, the specific heat at constant volume, $T_0=273.15\,\mathrm{K}$ a reference temperature, and $e_{l0}=617.0\,\mathrm{J\,kg^{-1}}$ a reference internal energy.

VAPOR PHASE

The equations of state for the vapor phase are considered based on a calorically perfect gas model. Therefore the corresponding equation for the pressure is

$$p_v(\rho_v, T_v) = \rho_v R T_v \tag{8}$$

and the caloric equation of state can be expressed as

$$e_v(T_v) = C_{vv}(T_v - T_0) + L_v(T_0) + e_{l0}, \tag{9}$$

where the constants with their corresponding values for water vapor are defined as: $L_v(T_0) = 2.3753 \times 10^6\,\mathrm{J\,kg{-}1}$ the latent heat of vaporization, $T_0 = 273.15\,\mathrm{K}$ the reference temperature, and $C_{vv} = 1410.8\,\mathrm{J\,kg^{-1}\,K^{-1}}$ the specific heat at constant volume.

MIXTURE PHASE

For the mixture phase it is assumed that the liquid and vapor phases are in mechanical and thermodynamic equilibrium. The equation of state for pressure is considered by taking the mixture pressure equal to the saturation pressure:

$$p_l = p_v = p_{sat}(T). \tag{10}$$

The mixture density can be written as

$$\rho = \alpha \rho_{v,sat}(T) + (1-\alpha)\rho_{l,sat}(T), \tag{11}$$

and the caloric equation of state for the mixture is defined by

$$\rho e = \alpha \rho_{v,sat}(T) e_v(T) + (1-\alpha)\rho_{l,sat} e_l(T) \tag{12}$$

where α is the void fraction of the vapor. The saturation parameters are functions of temperature and are obtained via the following curve fits [5].

$$\ln\left(\frac{p_{sat}(T)}{p_c}\right) = \frac{T_c}{T}\sum_{i=1}^{7} a_i \theta^{\hat{a}_i}, \tag{13}$$

$$\frac{\rho_{l,sat}(T)}{\rho_c} = \sum_{i=1}^{7} b_i \theta^{\hat{b}_i}, \tag{14}$$

$$\ln\left(\frac{\rho_{v,sat}(T)}{\rho_c}\right) = \sum_{i=1}^{7} c_i \theta^{\hat{c}_i}, \tag{15}$$

where $a_i, \hat{a}_i, b_i, \hat{b}_i, c_i, \hat{c}_i$ are constants (see [5] for the actual values). These functions are valid for ranges of temperature $T_r \le T \le T_c$, where T_r, and T_c are the triple point and critical point temperatures, respectively. The values of the constants used in the above expressions are $T_c = 647.16\,\mathrm{K}$, $p_c = 22.12 \times 10^6\,\mathrm{Pa}$, $\rho_c = 322.0\,\mathrm{kg\,m^{-3}}$, $T_r = 273.15\,\mathrm{K}$.

2 THERMODYNAMIC TABLES

The thermodynamic equations of state introduced in previous sections are highly nonlinear, especially for the mixture phase. By profiling the code used by Koop *et al.* [3] it was found that approximately 90% of the computational time was spent in the iterative algorithms used for solving these thermodynamic equations of states. To remove this bottleneck, thermodynamic tables are proposed in this paper. Considering the equations of state for the liquid, vapor, and mixture phases (equations (7), (9), and (12)), it can be shown that these equations give a unique relation between internal energy, temperature, density and pressure. Equation (12) can be written as

$$e(\rho, T) = \frac{\alpha\left(\rho_{v,sat} e_v - \rho_{l,sat} e_l\right) + \rho_{l,sat} e_l}{\rho} \tag{16}$$

For ρ, density of the mixture, the relation $\rho_{v,sat} \le \rho \le \rho_{l,sat}$ holds. Then from equation (16) we have $e\left(\rho_{l,sat}, T\right) = e_{l,sat} = e_l(T)$, and $e\left(\rho_{v,sat}, T\right) = e_{v,sat} = e_v(T)$. Hence, the caloric equations of state for liquid, vapor, and mixture phases imply the following inequality

$$e_l(T) \le e(\rho, T) \le e_v(T) \tag{17}$$

Therefore it is concluded that the caloric equations of state in the current study cover all the possible thermodynamic states consistently. In other words, the thermodynamic state of the system here is uniquely defined by the equations of state for liquid, vapor, and mixture. Figure 1 may help to create a visual insight into this expression. Due to uniqueness of thermodynamic equations of state, a thermodynamic table can be prepared covering data for desired variables in all the liquid, vapor, and mixture

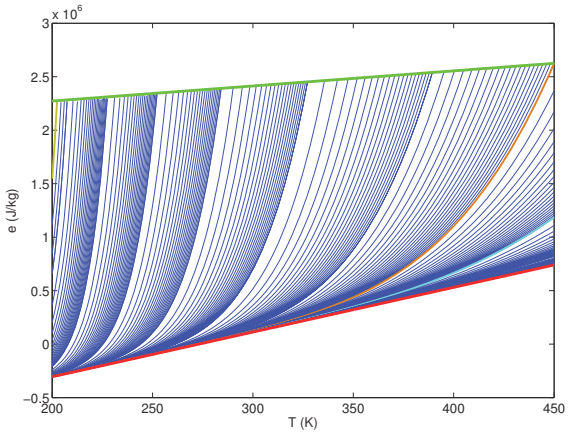

Figure 1. Sampling cross sections of plots for energy e versus temperature $200 \le T \le 450(\mathrm{K})$ with constant density ($2 \times 10^{-6} \le \rho \le 1100(\mathrm{kg\,m^{-3}})$). Green: saturation/vapor phase, red: saturation/liquid phase, blue: mixture phase, yellow: $\rho \approx 2 \times 10^{-4}(\mathrm{kg\,m^{-3}})$, brown: $\rho \approx 4.8(\mathrm{kg\,m^{-3}})$, cyan: $\rho = 20(\mathrm{kg\,m^{-3}})$

phases. Hence, a set of tables can be prepared containing data for the dependent variables based on known data from the thermodynamic pairings. In this study a set of tables has been prepared for $\Psi = \{T, p, c, \alpha\}$ based on a pairing (ρ, e), where c, and α denote the speed of sound and void fraction of vapor, respectively.

In a cavitating fluid the density range is varying from rather low densities (vapor) to high densities (liquid). Moreover, considering figure 1 it is observed that the ranges of energy can also possess very different values when comparing the parts with low densities to the ones with high densities. Therefore, preparing a single table for all the phases based on a thermodynamic pairing (ρ, e) with equal steps in the entire table (which is needed for an efficient look-up procedure) will be either inaccurate or very inefficient and costly. To deal with this problem, each table for the thermodynamic data was split into different regions with respect to density and the corresponding energy ranges. In order to keep consistency at the boundaries between regions of the table, an overlapping part is considered between neighboring regions. The interpolation in the overlapping part is carried out based on a weighted averaging of the interpolated data from the overlapping regions. Let indices m, and n represent two neighboring regions of the table with an overlapping region denoted by index mn. The density ranges are assumed as $\rho_m^a \leq \rho_m \leq \rho_m^b$, and $\rho_n^a \leq \rho_n \leq \rho_n^b$ for regions m and n, where superscripts a and b refer to the starting and ending values of the domain, respectively. The thermodynamic data in overlapping parts ($\rho_n^a \leq \rho_{mn} \leq \rho_m^b$) are obtained by a weighted averaging of their interpolated values in the overlapping regions. Let the thermodynamic data in overlapping part be Ψ_{mn}, then

$$\Psi_{mn} = \beta \Psi_m + (1-\beta)\Psi_n \tag{18}$$

where β is the averaging weight such that

$$\beta = \frac{\rho_{mn} - \rho_m^b}{\rho_n^a - \rho_m^b} \tag{19}$$

Figure 2, represents regions of the prepared tables and the values of the boundaries for each region. The overlapping parts between each two neighboring regions are clear from the same figure. The maximum relative error of interpolation for temperature is found to be of the order $O\left(10^{-4}\right)$ in the whole domain.

3 DISCRETIZATION METHOD

The governing equations (equation (1)) are solved using a cell-centered finite volume approach on multiblock structured grids. Dividing the physical domain in a set of non-overlapping non-deforming volumes V_i with boundary ∂V_i, and replacing the inter-cell flux by a numerical flux $\mathbf{H}$ which is assumed to be constant over face S_{ij}, the discretized form of the equations for each volume at time level t^n can be written as

$$\frac{\partial \bar{\mathbf{U}}_i}{\partial t} = -\Re_i, \tag{20}$$

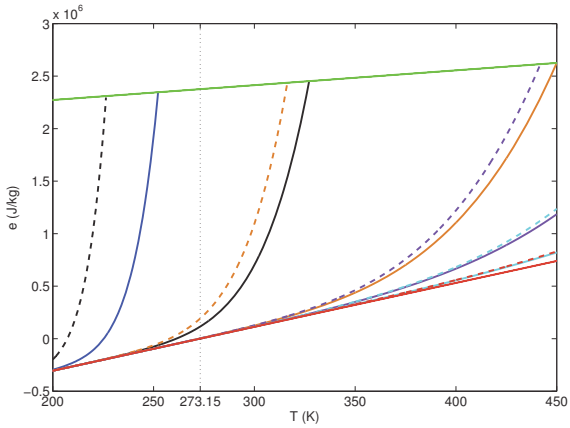

Figure 2. Regions of thermodynamic tables (6 regions), each region is defined between two solid and dashed lines of the same color. Blue: $2\times10^{-6} \leq \rho \leq 0.001(\mathrm{kg\,m^{-3}})$, black: $9\times10^{-4} \leq \rho \leq 0.1(\mathrm{kg\,m^{-3}})$, brown: $0.06 \leq \rho \lesssim 4.8(\mathrm{kg\,m^{-3}})$, violet: $4 \leq \rho \leq 20(\mathrm{kg\,m^{-3}})$, cyan: $18 \leq \rho \leq 100(\mathrm{kg\,m^{-3}})$, red: $90 \leq \rho \leq 1100(\mathrm{kg\,m^{-3}})$. Green and red lines represent saturation/vapor phase and saturation/liquid phase lines, respectively.

where

$$\bar{\mathbf{U}}_i = \frac{1}{|V_i|}\iiint_{V_i} \mathbf{U}\,\mathrm{d}\Omega \tag{21}$$

and $\Re_i$ is the spatial residual

$$\Re_i = \frac{1}{|V_i|}\sum_{j=1}^{N_{S,i}} \mathbf{H}\left(\mathbf{U}_L, \mathbf{U}_R, \mathbf{n_{ij}}\right)\left|S_{ij}\right|. \tag{22}$$

$\mathbf{U}_L$ and $\mathbf{U}_R$ are the variables on left and right sides of the volume's face and are determined via the MUSCL reconstruction technique [6]. The actual variables used for the reconstruction are density, three components of velocity and internal energy, i.e. $\{\rho, u, v, w, e\}$. This turned out to be a more stable reconstruction than using the conservative variables $\{\rho, \rho u, \rho v, \rho w, \rho E\}$, because for the latter it cannot be guaranteed that the internal energy is interpolated monotonically, which is crucial for the stability of the method.

For the numerical flux scheme $\mathbf{H}$ in equation (22) the AUSM+-up for all speeds ([7], [8]) is used. This flux scheme requires a cut-off Mach number for the correct treatment of the pressure in the low Mach number regime. The results shown in section 4 are obtained by choosing a cut off value of 0.01.

The discretized form of the equations for each cell at time level t^n can be written as

$$\frac{\partial \bar{\mathbf{U}}_i}{\partial t} = \Re\left(\mathbf{U}_i^n\right), \tag{23}$$

where $\Re(\mathbf{U}_i^n)$ is the residual at time t^n. The temporal discretization is carried out using a third order accurate three-stage TVD Runge-Kutta method ([9]). Assuming $\mathbf{U}_i^n$ the vector of variables at time step n, then $\mathbf{U}_i^{n+1}$ is obtained as shown below

$$\mathbf{U}_i^{(1)} = \mathbf{U}_i^n + \Delta t \Re(\mathbf{U}_i^n) \tag{24}$$

$$\mathbf{U}_i^{(2)} = \frac{3}{4}\mathbf{U}_i^n + \frac{1}{4}\mathbf{U}_i^{(1)} + \frac{1}{4}\Delta t \Re(\mathbf{U}_i^{(1)}) \tag{25}$$

$$\mathbf{U}_i^{n+1} = \frac{1}{3}\mathbf{U}_i^n + \frac{2}{3}\mathbf{U}_i^{(2)} + \frac{2}{3}\Delta t \Re(\mathbf{U}_i^{(2)}) \tag{26}$$

For cavitating flows the time step Δt must be taken very small such that the details of the propagation of pressure waves are resolved. Furthermore at each time step the CFL condition is checked using the following definition,

$$C = \Delta t \frac{max(|\mathbf{u_i}| + c_i, |\mathbf{u_i}|)}{\ell_i}. \tag{27}$$

where C is the CFL number, and ℓ_i the characteristic length of the cell.

4 RESULTS

The physical model in combination with the thermodynamic models and the spatial discretization described above has been tested for the unsteady 2D cavitating flow around a NACA0015 at 6^o angle of attack. This is a standard test case, which has also been computed by Sauer & Schnerr [10], Schnerr *et al.* [11] and Koop [2]. In contrast to the references above tunnel walls have not been included. Furthermore a non-reflecting boundary condition treatment has not yet been implemented at this stage of the research. Instead a farfield boundary is used with the farfield located 900 chord lengths away. A picture of the O-type grid used is shown in figure 3. It consists of 256 cells around the airfoil and 72 cells normal to the airfoil. An accuracy study for the fully wetted flow case, not included in this paper, indicated that this resolution was sufficient to obtain grid converged values for the lift coefficient. It has been assumed that this grid was also fine enough for an accurate representation of the cavitation case, although the authors realize that much more complicated physics is involved when cavitation is occurs.

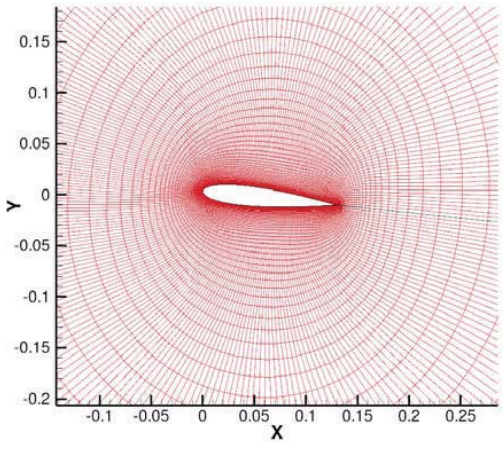

Figure 3. Detail of computational grid around the NACA0015 hydrofoil. The grid consists of 256 cells around the airfoil and 72 cells normal to the airfoil

U_∞ [m s^{-1}]	p_∞ [10^5Pa]	T_∞ [K]	ρ_∞ [kg m^{-3}]	c_∞ [m s^{-1}]	σ [–]
50	12.5	293	998.7	1540.0	1.0

Table 1. Conditions for the cavitating flow around the 2D NACA0015 hydrofoil at 6^o angle of attack with chord length $c = 0.13$m.

Following Koop [2] the free-stream velocity has been increased to speed up the shedding process. However, the cavitation number σ is kept the same compared to the original conditions, hence also the free-stream pressure has been increased. A summary of the conditions can be found in table 1.

The initial solution for the unsteady cavitating flow is the steady, fully wetted flow solution obtained using the modified Tait equation, see section 1. In order to guarantee a monotonic solution, the MinMod limiter is employed in the MUSCL reconstruction, see section 3. A time step of 10^{-9} seconds was chosen, such that all physical phenomena could be captured. A total of 16 million time steps were carried out, which took approximately 60 hours of computing time on 12 processors (Intel Xeon X5650 @ 2.67GHz).

Figure 4 shows the void fraction at six different time instances, where the time between each of the figures is 0.0005 seconds. The shedding of the vapor cloud is clearly visible in these figures. Furthermore, figures 4(d), 4(e) and 4(f) show the formation of the attached sheed cavity and the appearance of the reentrant jet, leading to the formation of the next vapor cloud.

When the vapor region, which contains vorticity, passes the trailing edge of the airfoil, vorticity of opposite sign is generated at the trailing edge, leading to a change in the force experienced

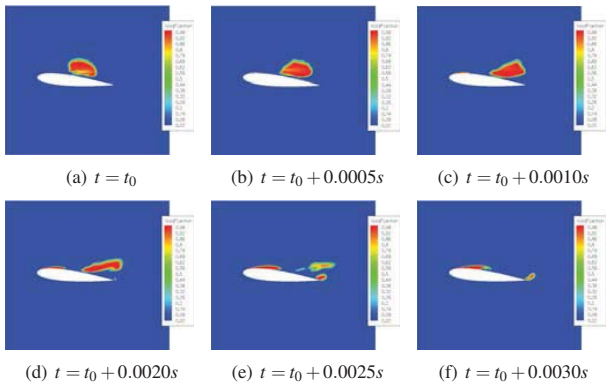

(a) $t = t_0$ (b) $t = t_0 + 0.0005s$ (c) $t = t_0 + 0.0010s$

(d) $t = t_0 + 0.0020s$ (e) $t = t_0 + 0.0025s$ (f) $t = t_0 + 0.0030s$

Figure 4. Void fractions at different time instances for the cavitating flow over the NACA0015 hydrofoil at 6^o angle of attack, $\sigma = 1.0$

.

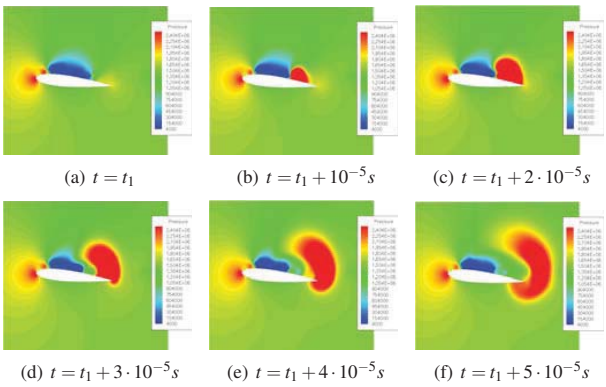

(a) $t = t_1$ (b) $t = t_1 + 10^{-5}s$ (c) $t = t_1 + 2 \cdot 10^{-5}s$

(d) $t = t_1 + 3 \cdot 10^{-5}s$ (e) $t = t_1 + 4 \cdot 10^{-5}s$ (f) $t = t_1 + 5 \cdot 10^{-5}s$

Figure 5. Pressures at different time instances for the cavitating flow over the NACA0015 hydrofoil at 6^o angle of attack.

.

by the hydrofoil. The vorticity at the trailing edge is so intense that the flow cavitates.

In figure 5 an image sequence of the pressure is depicted. The time interval between these images is 10^{-5} seconds, i.e. 50 times smaller than the time interval shown in figure 4. It is clear that the thermodynamic cavitation model used in this work is able to predict the collapse of the vapor cloud and the corresponding formation of a shock wave. As the time intervals between the pressure pictures is only 10^{-5} seconds, this shows that this phenomenon takes place at a much smaller time scale than the shedding of the vapor clouds.

The region with high pressure (maximum pressure around 80 bar, at least in the used sampling rate of 5 microseconds) is generated at the moment the shed vapor region collapses just upstream of the trailing edge. Following the collapse a shock wave is formed which propagates outwards and rebounds from the hydrofoil's upper surface as well as the upstream vapor region. The shock front also curls around the trailing edge and propagates upstream along the hydrofoil's lower surface.

5 CONCLUSIONS AND FUTURE WORK

For the equilibrium cavitation model developed by Saurel *et al.* [4] and Schmidt *et al.* [1] thermodynamic tables for all three phases, liquid, vapor and mixture, have been presented. The analytical expressions for the thermodynamic closure relations, which are computationally intensive [2], have been replaced by tables containing the same information. By splitting the table in subtables, with each equidistant spacing, an efficient look-up procedure can be used, which hardly requires any computational time. Consequently a speed-up of approximately a factor of 10 can be obtained compared to the original method of by Koop [2].

The robustness of the approach have been shown by simulating the cavitating flow around the 2D NACA0015 hydrofoil at 6^o angle of attack. In the results the formation of the sheet cavity of the reentrant jet can clearly be seen as well as shedding and the collapse of the vapor region.

Future work to be carried out is the extension of the method to viscous flows using the LES approach for modeling effects of turbulence and apply the method to vortex cavitation. Furthermore, it is worthwhile to investigate whether implicit time stepping techniques are useful for this type of application. In the simulation shown in section 4 the time step is 10^{-9} seconds. When the extension to viscous flow is made, the time step must be reduced even further for stability reasons, especially when finer grids are employed. On the other hand, a time step of approximately 10^{-6} seconds may be sufficient to capture the physics of pressure waves. If this is indeed the case, implicit time integration methods will be significantly more efficient than their explicit counterparts.

ACKNOWLEDGMENTS

This research is carried out under the sponsorship of AgentschapNL in the framework of the Maritime Innovation Program, MIP-IOP IMA 09009.

REFERENCES

[1] Schmidt, S.J., Sezal, I.H., and Schnerr, G.H., 2006. "Compressible Simulation of High-Speed Hydrodynamics with Phase Change". *ECCOMAS CFD*.

[2] Koop, A., 2009. "Numerical Simulation of Unsteady Three-Dimensional Sheet Cavitation". PhD thesis, University of Twente, the Netherlands.

[3] Koop, A., and Hoeijmakers, H., 2009. "Numerical Simulation of Unsteady Three-Dimensional Sheet Cavitation". *Cav2009 Proceedings, Ann Arbor, Michigan, USA*, Aug.

[4] Saurel, R., Cocchi, J.P., and Butler, J.B., 1999. "A Numerical study of Cavitation in the Wake of a Hypervelocity Underwater Profile". *Journal of Propulsion and power. 15(4):513-522*.

[5] Schmidt, E., Sezal, I.H., and Schnerr, G.H., 1989. "Properties of Water and Steam in SI-Units; 0-800C, 0-1000 bar". *Springer-Verlag. R. Oldenbourg, 4th, enlarged printing edition*.

[6] Leer, van B., 1979. "Towards the Ultimate Conservative Difference Scheme V. A Second-order Sequel to Godunov's Method". *Journal of Computational Physics, 32:101-136*.

[7] Liou, M. S., 1996. "A Sequel to AUSM: AUSM+". *Journal of Computational Physics, 129:364382*.

[8] Liou, M. S., 2006. "A sequel to AUSM, Part II: AUSM+-up for all speeds". *Journal of Computational Physics, 214:137170*.

[9] Shu, C.-W., 1988. "Total - Variation - Diminishing time discretizations". *SIAM J. Scientific and Statistical Computing, 9, pp. 1073-1084*.

[10] Sauer, J., and Schnerr, G. H., 2000. "Unsteady Cavitating Flow - A New Cavitation Model Based on a Modified Front Capturing Method and Bubble Dynamics". *Fluids Engineering Summer Conference, Proceedings of FEDSM00*.

[11] Schnerr, G. H., Schmidt, S. J., Sezal, I. H., and Thalhamer, M., 2006. "Schock and Wave Dynamics of Compressible Liquid Flows with Special Emphasis on Unsteady Load on Hydrofoils and on Cavitation in Injection Nozzles". *Proceedings CAV2006, Sixth International Symposium on Cavitation, Wageningen, The Netherlands*.